Applicability of Dynamic Inflow Models of HAWT in Yawed Flow Conditions

Hur, C.; Ferreira, Carlos; Schepers, Gerard

DOI
10.3390/en15249368

Publication date
2022

Document Version
Final published version

Published in
Energies

Citation (APA)
Hur, C., Ferreira, C., & Schepers, G. (2022). Applicability of Dynamic Inflow Models of HAWT in Yawed Flow Conditions. *Energies*, *15*(24), Article 9368. https://doi.org/10.3390/en15249368

energies

MDPI

Article

Applicability of Dynamic Inflow Models of HAWT in Yawed Flow Conditions

Chihoon Hur [1,*,†], Carlos Ferreira [1] and Gerard Schepers [2]

[1] Faculty of Aerospace Engineering, Delft University of Technology, Kluyverweg 1, 2629 HS Delft, The Netherlands
[2] TNO Energy Transition, Wind Energy, 1755 LE Petten, The Netherlands
* Correspondence: c.hur@iae.re.kr or chihoonhuh@gmail.com
† Current address: Institute for Advanced Engineering, Goan-ro 51beon-gil, Yongin-si 17180, Gyeonggi-do, Republic of Korea.

Abstract: Horizontal axis wind turbines (HAWTs) experience yaw misalignments due to the physical limitations of yaw controllers and various novel active yaw controls. Moreover, the motion of floating offshore wind turbines (FOWTs) accelerates yaw misalignment. The blade element momentum (BEM) method is widely used due to its computational efficiency for the design of HAWTs. Momentum theory, the basis of BEM, assumes steady flow and uniform induction field at the disc. Those assumptions are relaxed by engineering models to capture yaw and unsteady effects. Current yaw engineering models, however, are inaccurate since they do not capture the asymmetric wake expansion effect. Dynamic inflow models have been developed for non-yawed flow. Furthermore, the AVATAR project shows that BEM using fully coupled engineering models, the current yaw, dynamic inflow and various engineering models, suffers from significant deficiencies. This purpose of this paper, therefore, is to investigate dynamic effects for yawed flow, and determine if current dynamic inflow models are applicable in yawed conditions. The Glauert's modified momentum theory is applied to dynamic inflow models to couple the two models. Among all coupled models, Øye, Yu PWVM and Yu FWVM DIM can capture asymmetric trends. However, the results show the significant deficiencies in phase delay on the actuator disc.

Keywords: horizontal axis wind turbines; actuator disc; yaw; dynamic inflow; BEM; vortex; CFD

Citation: Hur, C.; Ferreira, C.; Schepers, G. Applicability of Dynamic Inflow Models of HAWT in Yawed Flow Conditions. *Energies* **2022**, *15*, 9368. https://doi.org/10.3390/en15249368

Academic Editors: Hwachang Song and Hyun-Goo Kim

Received: 31 October 2022
Accepted: 8 December 2022
Published: 10 December 2022

1. Introduction

Horizontal axis wind turbines (HAWTs) experience yaw misalignments due to the continuous change of wind direction and the limitations of yaw controllers. Various novel approaches to utilize active yaw control have been introduced in order to maximize power production [1–3], resulting in more frequent exposures to yaw misalignment. Moreover, the motion of floating offshore wind urbines (FOWTs) accelerates yaw misalignment [4]. The yaw misalignment cause complex dynamic effects; in particular, periodic loads on wind turbines play a role in fatigue and extreme loads [5,6]. The blade element momentum (BEM) method is widely used due to its computational efficiency for the design of wind turbines. BEM makes it possible to calculate extreme and fatigue loads over 10,000 single design load cases (DLCs) for the life time of floating offshore wind turbines [7].

Momentum theory is the basis of BEM, assuming steady flow and uniform induction field at the disc. Those assumptions are relaxed by engineering models to capture unsteady and yaw effects. However, current yaw momentum engineering models are inaccurate since they do not consider asymmetric wake expansion effects [8]. Rahimi also highlighted that significant deviations of the current yaw engineering models occur for yawed flow [9]. Dynamic inflow models are developed for non-yawed flow [10]. However, the combined dynamic wake model for yawed flow has not been introduced yet, and in the AVATAR project, fully coupled aero-elastic tools are simulated, using 10 different engineering models,

including yaw and dynamic inflow models. Results from the project show that BEM has significant deficiencies. Therefore, further investigation is required on the dynamic effects for yawed flow. In this paper, an actuator disc was modeled using current engineering models and compared against the high fidelity CFD approach for yawed flow with dynamic loading. Dynamic phenomena in yaw were also evaluated at different yaw angles and varying thrust coefficients at the different location of the actuator disc.

2. Description of Models

Wind turbines are represented as an actuator disc in the paper, assuming an infinite number of blades and rotational speed. Therefore, the effects of tip loss and rotational speed are neglected. The uniformly distributed load is applied to the actuator disc, de-accelerating incoming velocity in upwind part as seen in Figure 1. In yawed conditions, the lateral force of the actuator disc pushes the flow on the y-axis, resulting in vorticities not only in the azimuthal direction, but also in the longitudinal direction. The vorticities in the longitudinal direction cause a kidney shape in their wake as shown in the Figure 1. The causes of kidney-shaped and skewed wake are well-described in Berdowski's work [11]. In this paper, the induction field will be more focused on investigating the dynamic effects at the actuator disc in yaw.

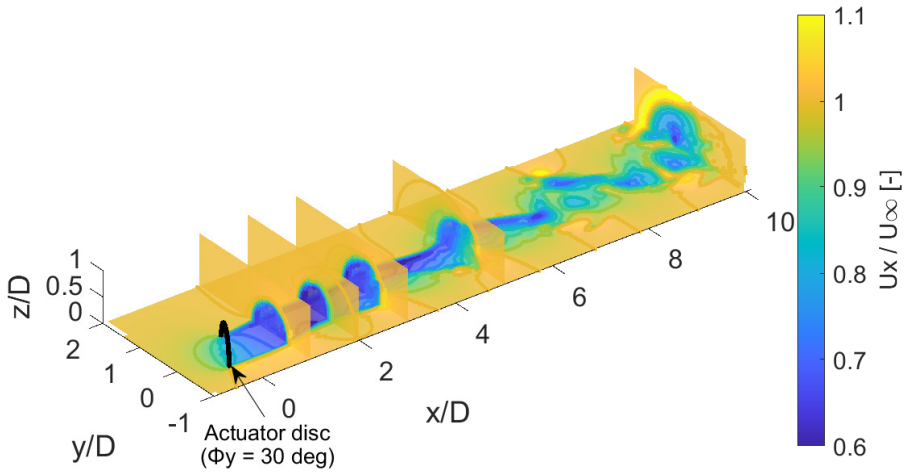

Figure 1. The upper part of the actuator disc and normalized velocity field around disc and in the wake, when base $C_T = 0.6$, harmonic $\Delta C_T = \pm 0.1$, $\Phi_y = 30$ deg, $f_r = 0.1$, where C_T is the trust coefficient, ΔC_T is the change of the trust coefficient, Φ_y is the yaw angle, and f_r is the reduced frequency $\left(\frac{\omega R}{U}\right)$.

2.1. Engineering Models

2.1.1. Yaw Momentum Engineering Models

Yaw momentum models are explained in the literature [8]. Among various yaw engineering models, Øye's model is selected since this model can predict the non-linear radial dependency of induction field.

2.1.2. Dynamic Inflow Engineering Models

Various state-of-the-art dynamic engineering models—Pitt–Peters [12], ECN [13], Øye [14], and Yu (linear and non-linear approach) models [10]—are implemented to evaluate them with a numerical 3-dimensional CFD model for non-yawed and yawed flow. The detailed descriptions of the models are provided in Yu's work [10].

2.1.3. Coupling Yaw and Dynamic Inflow Engineering Models

In order to couple yaw and dynamic inflow models, the modification of dynamic inflow model is necessary. Current dynamic inflow models assume the momentum balance

which is $C_T = 4a(1-a)$, where a is the induction factor, and this assumption is not valid for yawed flow [8]. For yawed flow, the momentum relation is described in Equation (1), which was suggested by Glauert [15].

$$C_T = 4a\sqrt{1-a(2cos\Phi_y - a)} \tag{1}$$

Therefore, Pitt–Peters and ECN dynamic inflow models need to be modified as Equations (2) and (3) below. Those differential equations satisfy Glauert's modified momentum theory as Equation (1).

- Modified Pitt–Peters' dynamic inflow model:

$$\frac{da}{dt} = \left(\frac{C_T}{4} - a\sqrt{1-a(2\cos\Phi_y - a)}\right) / \frac{4r}{3\pi} \tag{2}$$

- Modified ECN dynamic inflow model:

$$\frac{da}{dt} = \left(\frac{C_T}{4} - a\sqrt{1-a(2\cos\Phi_y - a)}\right) / \frac{Rf_a}{U_0} \tag{3}$$

Here, the term, f_a, which is defined as Equation (4), obtains radial dependency effects:

$$f_a = 2\pi / \int_0^{2\pi} \frac{1-(r/R)\cos\phi_r}{[1+(r/R)^2 - 2(r/R)\cos\phi_r]^{3/2}} d\phi_r \tag{4}$$

- Øye dynamic inflow model for yawed flow

Øye suggested that the dynamic inflow model consists of two first-order linear differential equations as Equations (5) and (6). Here U_{qs} is the term for quasi-steady responses, which enables us to apply the modified Glauert's momentum theory in Equation (1):

$$\frac{dU_{int}}{dt} = \left(U_{qs} + \kappa\tau_1 \frac{dU_{qs}}{dt} - U_{int}\right) / \tau_1 \tag{5}$$

U_{int} is an intermediate value. And the κ is 0.6. Therefore, once the quasi-steady responses are determined for yawed flow, Øye's dynamic inflow model does not need to be modified:

$$\frac{da}{dt} = (U_{int} - a)/\tau_2 \tag{6}$$

The two time constants tau_1 and tua_2 are calibrated based on the prescribed vortex ring model which is introduced in literature [14], and Snel and Schepers [16] suggested the time constants as Equations (7) and (8). Yu also explained Øye dynamic inflow model in her PhD thesis [17]:

$$\tau_1 = \frac{1.1}{(1-1.3a)} \frac{R}{U_0} \tag{7}$$

$$\tau_2 = (0.39 - 0.26(\frac{r_j}{R})^2)\tau_1 \tag{8}$$

where the r_j indicates the radial position.

- Yu dynamic inflow model for yawed flow

Yu [10] introduced two dynamic inflow models, a linear and a non-linear dynamic inflow model based on the prescribed vortex tube model and free wake vortex ring model, respectively. Using two vortex models, the indicial step responses of the induction field are represented by an exponential approximation. The ϕ is the indicial function as described in Equation (9):

$$\phi(t) = 1 - \beta e^{\omega_1 t} - (1-\beta)e^{\omega_2 t} \tag{9}$$

where, β, ω_1, ω_2 are indicial coefficients as a function of thrust coefficients and the position of the actuator disc, obtained by the least-square approach. The coefficients are determined

based on the database set, using 2 parameters as recommended by Pirrung and Madsen [18] and Yu [10]. The indicial coefficients and detailed description are given in Yu's literature [10].

The two dynamic inflow models can be also applied for yawed flow by changing the momentum relation to modified momentum balance as Equation (1) introduced by Glauert [19]. The indicial coefficients introduced in Equation (9) are determined by modified momentum relation in the Equation (1).

It is noted that dynamic inflow models and yaw models have an apparent contradiction since the assumption of the dynamic inflow model is an axis-symmetric flow, which is not the case for yawed conditions. This raises the question of whether coupled dynamic and yaw engineering models are applicable for fully coupled analysis.

2.2. Vortex Models

Prescribed and Free Wake Vortex Models

The prescribed wake vortex model (PWVM) [8] and free wake vortex model (FWVM) [11] developed by TUDelft are used to assess the yaw effects and to verify the models. The description of vortex models is explained in ref. [8].

2.3. 3-Dimensional Actuator Disc CFD Modeling

Assuming that the upper and lower parts of the disc have the same phenomena, the upper half of a 3-dimensional actuator disc is modeled. The length, width and height of the control volume domain are 40D, 20D and 10D, respectively. The region of the actuator disk and wake are refined by the Snappy–Hex approach provided in OpenFOAM (Open source Field Operation And Manipulation) tool box. The model consists of approximately 7 million cells. Unsteady solver for incompressible flow, pisoFOAM in the OpenFOAM tool box, is used. The flow is assumed to be laminar. Sørenson proves that the laminar flow at a low Reynolds number sufficiently represents the induction field of the actuator disc [20]. The time step of the simulations is 0.00025τ.

Convergence Study

A convergence study of the CFD model was performed for steady flow cases in order to compare it against momentum theory when $C_T = 0.6$ and $\Phi_y = 0$ deg. Due to the discontinuity of pressure at the actuator disc, the axial induction factor at the disc is not constant. The induction factor very close to the disc from $x/D = -0.05$ to 0.05 shows a linear trend, except the jump. Therefore, the induction field at the disc will be linearly interpolated. For the convergence study, axial induction factor a_n in the far wake where $x/D = 25$, $y/D = 0$, and $z/D = 0$, is selected. As shown in Table 1, the axial induction factor in the far wake is slightly lower than momentum theory. The maximum gap is approximately 0.25%. In this research, the mesh of Case No. 3 is selected for simulations.

Tabel 1. Convergence study for different mesh resolutions where $C_T = 0.6$, $\Phi_y = 0$ deg.

Case No.	N_x	N_y	N_{cell}	$2 \times a_n$ CFD	Ratio Case 1/Case 8	$2 \times a_n$ Momentum Theory
1	120	38	1 milion	0.3686	99.68%	0.3675
2	160	38	1.5 milions	0.3686	99.68%	0.3675
3	160	80	6.6 milions	0.3669	99.95%	0.3675
4	400	80	15 milions	0.3669	99.95%	0.3675
5	400	150	27 milions	0.3666	100.00%	0.3675
6	400	200	34 milions	0.3665	100.01%	0.3675
7	600	200	50 milions	0.3666	100.01%	0.3675
8	800	200	67 milions	0.3666	100.00%	0.3675

2.4. Verification of Models

Several models—momentum models and fixed and free wake vortex models [11]—are compared with CFD model for non-yawed steady flow in order to verify the models as shown in Figure 2.

All the models match well where $C_T <= 0.6$, while induction factor a_n from the free wake vortex model and CFD model is lower at higher C_T. It is interesting that the prescribed wake vortex model agrees with momentum theory well, whereas the free wake vortex model predicts a lower induction factor at higher thrust coefficient, although both vortex models follow same approach [8]. The reason is that the free wake vortex model is able to consider the wake expansion effect so that the vorticity generated near the edge of the disc is further than the vorticity from the prescribed wake vortex model. This causes a lower induction factor, especially at the center of the disc as illustrated in Figure 2. Base C_T is determined as 0.6, since the value is the highest where results from all the models are likely to have good agreements as seen in Figure 2.

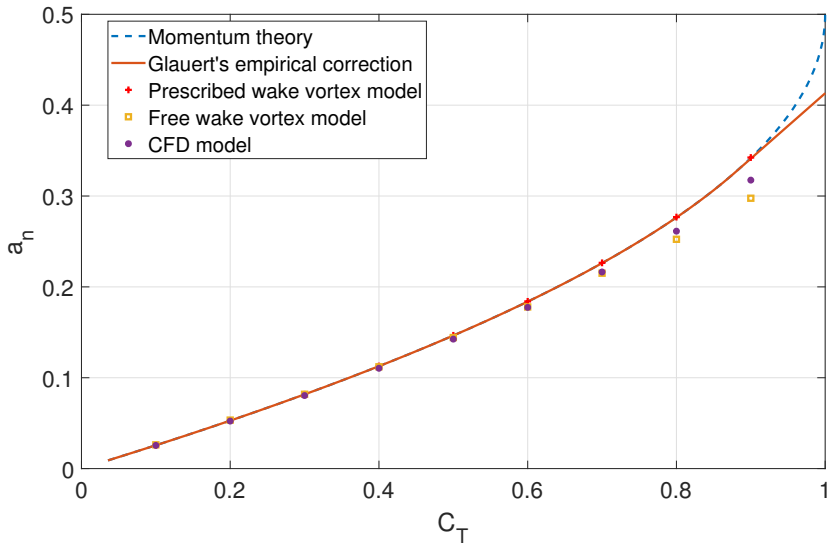

Figure 2. Comparison of momentum balance with different models at the center point of actuator disk where z/R = 0, y/R = 0 and yaw angle = 0 deg.

3. Case Studies

Operation Conditions

Using state-of-the-art engineering models, the vortex and CFD models explained in Section 2, induction fields are computed at different yaw angles and varying loads as described in Table 2. Base C_T is determined as 0.6, because 0.6 is the highest value where the induction factor at the center of disc from all the models matches well, as illustrated in Figure 2. The yaw angle for the simulations is set as 30 deg to see the skewed wake effects more clearly [21]. Simulations are divided into four categories as explained in Table 2. Firstly, Cases I and II are simulated to validate the current models for non-yawed and yawed flow, respectively. Then case III and IV are calculated to predict dynamic load effects for non-yawed and yawed flow, respectively.

Tabel 2. Description of simulation cases.

	Case I	**Case II**	**Case III**	**Case IV**
Base C_T	0.6			
Load type	Constant load		Step load (ΔC_T = +0.1)	
Yaw angle	0 deg	30 deg	0 deg	30 deg
Models	Øye yaw model (YM), PWVM, FWVM, CFD model		Pitt–Peters dynamic inflow model (DIM), ECN DIM, Øye's DIM, Yu PWVM (linear) DIM, Yu FWVM (non-linear) DIM CFD model	

4. Results and Discussion

4.1. Induction Field with Constant Load

The induction fields of an actuator disc with constant load are calculated from different models: Øyeś model, prescribed wake vortex model, free wake vortex model, and CFD model for non-yawed (Case I) and yawed flows (Case II).

4.1.1. Case I: Non-Yawed Flow and Constant Load

Øyeś model, one of the momentum engineering models, shows uniform induction field at the disc, whereas the vortex models and CFD model capture the non-uniform induction field. The non-uniformity of the induction field at the disc has already been proved by Sørenson [22]. Kuik also suggested a correction model for the non-uniform induction field as a function of C_T and radial position in his work [23]. Momentum models assume one-dimensional flow; however, as seen in Figures 3 and 4, the 3-dimensional induction fields interact with each other. This indicates the importance of understanding 3-dimensional phenomena at the disc. The edge part of induction fields from two vortex models is multiplied by a Gaussian core to deal with the singularity of vorticity [8], resulting in the sharp decrease in the induction field.

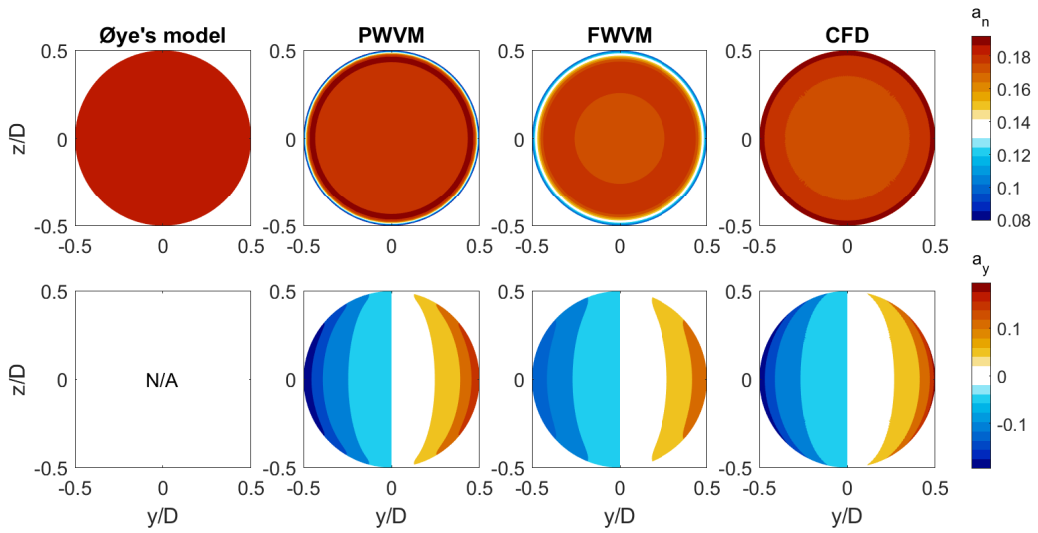

Figure 3. Induction field at the actuator disc on the axis normal to disc and y axis from different models when yaw angle = 0 deg and C_T = 0.6.

4.1.2. Case II: Yawed Flow and Constant Load

The 3-dimensional induction fields for yawed conditions are analyzed based on the momentum models and vortex models in the literature [8]. In this section, those models are compared with the CFD model. Figure 4 shows that the CFD model predicts more reasonable results at the edge of the actuator disc, as vortex models suffer from the numerical singularity at the edge of the disc [8] as explained in the earlier section. The reason that the free wake vortex model shows the lowest induction field is because the wake is not fully developed. It should be noted that the initial induction fields of steady state from different models are different, which might affect the phase delay of the induction field.

4.2. Induction Field with Dynamic Load

The non-dimensional induction fields of an actuator disc with step load ($\Delta C_T = +0.1$) at base $C_T = 0.6$ are calculated using different models: Pitt–Peters, ECN, Øye, Yu's two engineering models, and CFD model for non-yawed (Case III) and yawed flows (Case IV).

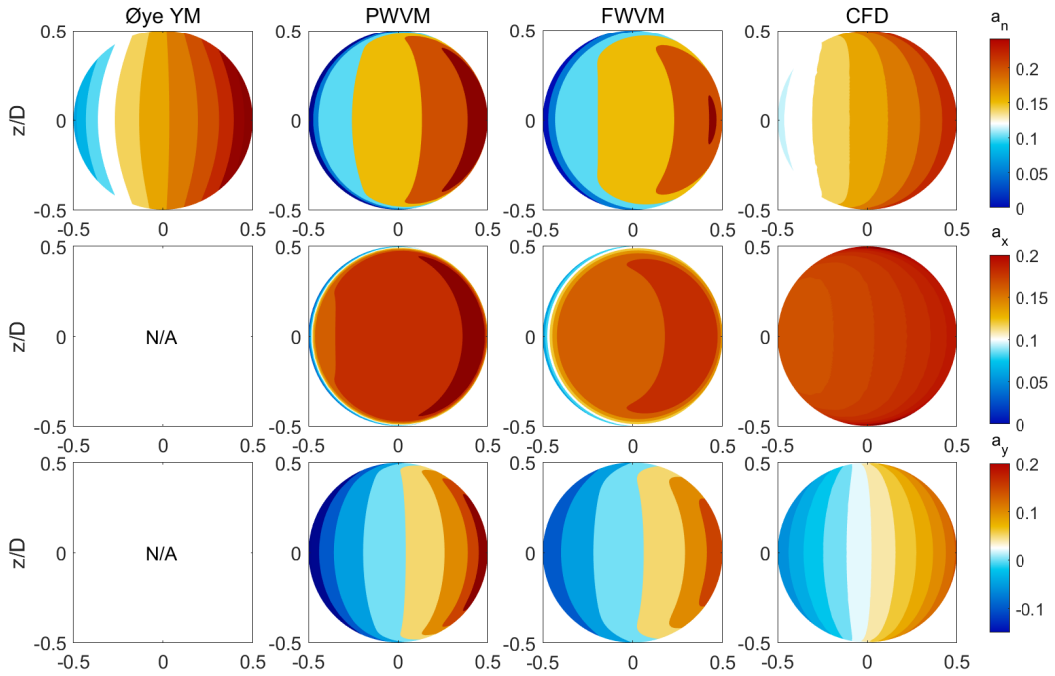

Figure 4. Induction field at the actuator disc on the axis normal to disc, x axis and y axis from different models when yaw angle = 30 deg and C_T = 0.6.

4.2.1. Case III: Non-Yawed Flow and Dynamic Load

Yu compared the current dynamic inflow models—Pitt–Peters, ECN, and Øye's engineering models—against vortex models and the 2-dimensional CFD model [10]. She proposed a new dynamic inflow model in her literature based on linear and non-linear actuator disc vortex models. Those models are implemented and compared with the three dimensional CFD model in Figure 5. All the dynamic inflow models estimate phase delay faster than the CFD results. Yu's model based on free wake vortex models matches well with the CFD result near the center of the disc as shown in Figure 5a; however, Figure 5c indicates that the CFD results show faster phase delay than Yu's non-linear model on the outer part of the disc. Note that the flow is assumed as axis-symmetric for non-yawed flow.

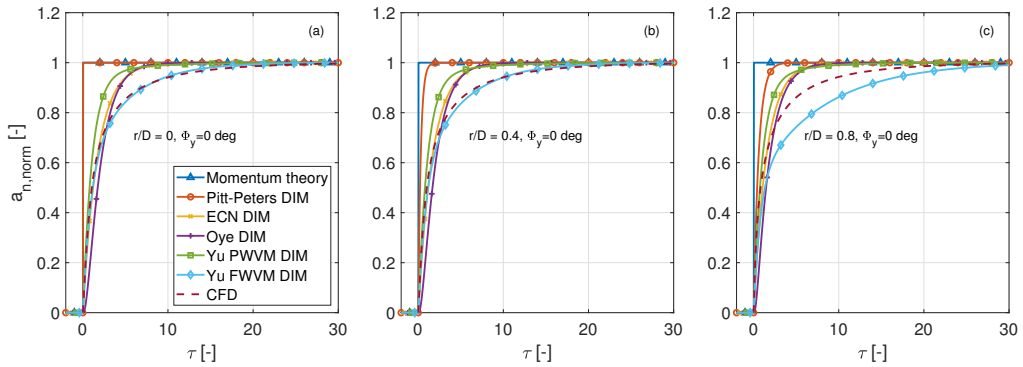

Figure 5. Normalized induction factor $a_{n,norm}$ at different positions when base C_T = 0.6, step ΔC_T = +0.1, Φ_y = 0 deg, (**a**) r/D = 0 (**b**) r/D = 0.4 (**c**) r/D = 0.8, τ is Non-dimensionalized time $\left(\frac{tU_0}{R}\right)$.

4.2.2. Case IV: Yawed Flow and Dynamic Load

The non-dimensional induction field where z/D = 0 is selected, where yaw effects are the most significant. Since current dynamic inflow models assume axis-symmetric flow, the dynamic inflow models are modified as described in Section 2.1.3. The two points of induction fields from those models in the downwind part (θ_{az} = 0 deg) and upwind part (θ_{az} = 180 deg) are the same as those seen in Figure 5a,c. On the other hand, the CFD results

show a different trend with respect to radial position (r/R) and azimuth angle (θ_{az}) as shown in Figure 6. Because the downwind part of an actuator disc is deeper in the wake, the phase delay is slower than the upwind part as seen in Figure 6. Figure 6c shows a relatively slower phase delay in the downwind part of the actuator disc. The development of wake for yawed flow with dynamic load is described in Figure 1. The flow is asymmetric due to the force in the lateral direction on the disc. Therefore, the time phase varies depending on redial positions and azimuth angles. This implies that it is required to create a new dynamic inflow model in yaw to take the dynamic asymmetric wake development into account.

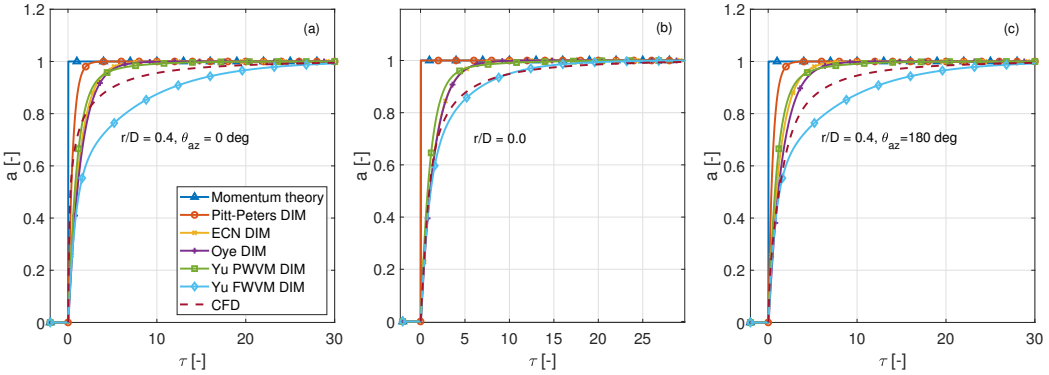

Figure 6. Normalized induction factor $a_{n,norm}$ at different positions when base C_T = 0.6, step ΔC_T = +0.1, Φ_y = 30 deg, (**a**) downwind part: r/D = 0.4, θ_{az} = 0 (**b**) center part: r/D = 0 (**c**) upwind part: r/D = 0.4

4.3. Analysis of Step Responses for Yawed Flow

4.3.1. Azimuth and Yaw Angle Dependency

To describe 3-dimensional dynamic phenomena at the actuator disc, the time derivatives of induction factors $da_x/d\tau$, $da_y/d\tau$ and $da_n/d\tau$ from the CFD model are plotted in Figures 7–9 at varying azimuth and yaw angles. Time derivatives of the induction factor on the z axis are not explained since they are converged into zero, which indicates that the dynamic effect on the z axis is negligible for yawed flow. Dynamic phenomena on x and y axis are the focus.

Figure 7 shows the time derivative of a_x. In the upwind part, the amplitude of the change of a_x is larger and the phase delay is faster. Those trends are clearly seen in larger yaw angles as seen in Figure 7b,c. The reason is that at the early stage of the step load, vorticities in the upwind part become closer to the actuator disc. On the other hand, vorticities in the downwind part become further away, resulting in a slower state change. In particular, in the case of Φ_y = 45 deg, the peak of the time derivative in the upwind part is sharp as described in Figure 7a. On the other hand, the time derivative in the downwind part is relatively extremely slower as shown in Figure 7c. The downwind part of the actuator disc is located in a deeper wake, induced by vorticities in both the downwind and upwind parts. At the beginning vorticities in downwind part is dominant, then the vorticities in the upwind part start to contribute more to slower phase delay as seen in Figure 7.

The time derivative of a_y shows a contrasting trend in the upwind and downwind parts as shown in Figure 8. Figure 8a,b describe the induction factor on the y axis in the downwind and center parts, showing the flow accelerated to the positive y axis, and then it becomes a steady state. On the other hand, the flow in the upwind part is accelerated to the positive y axis first at the beginning of the step load, after which it is decelerated, at last becoming a steady state. It seems that at the early stage of the step load, the force on the y axis is dominant, resulting in the sharp acceleration of a_y. Then the wake expansion effect becomes dominant, contributing to the acceleration of flow to the negative y axis in the downwind part. Figure 8c proves that this trend is clearer for a higher yaw angle. The time derivative of a_y increases significantly for higher yaw angles.

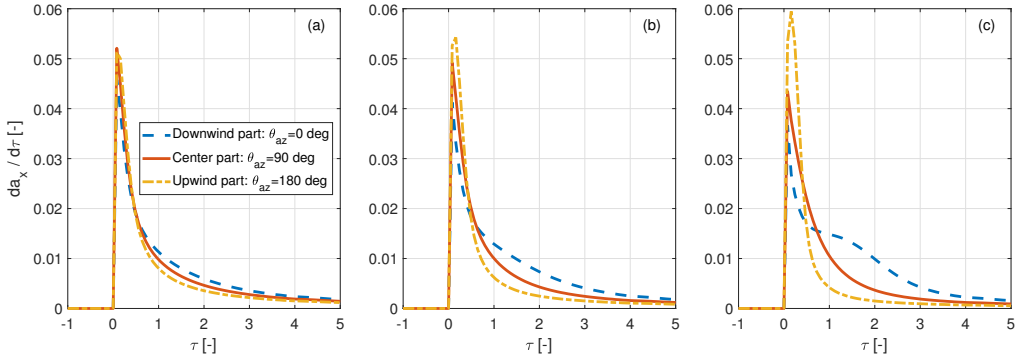

Figure 7. Time derivative of a_x at different azimuth angles from CFD model when base $C_T = 0.6$, step $\Delta C_T = +0.1$, r/D = 0.4, (**a**) $\Phi_y = 15$ deg, (**b**) $\Phi_y = 30$ deg, (**c**) $\Phi_y = 45$ deg.

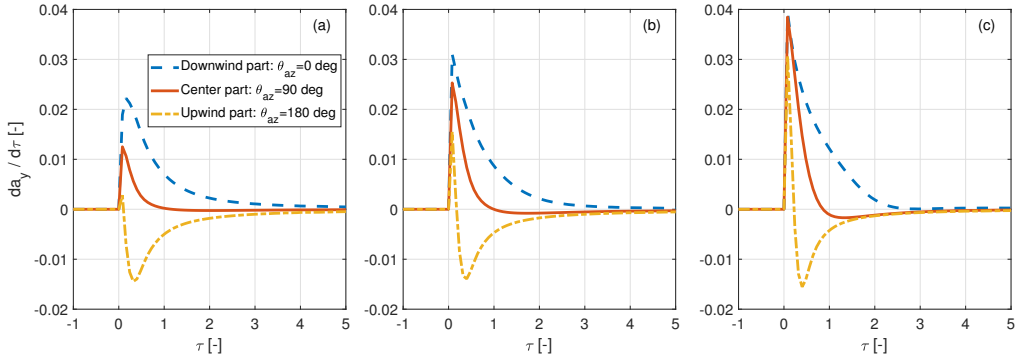

Figure 8. Time derivative of a_y at different azimuth angles from CFD model when base $C_T = 0.6$, step $\Delta C_T = +0.1$, r/D = 0.4, (**a**) $\Phi_y = 15$ deg, (**b**) $\Phi_y = 30$ deg, (**c**) $\Phi_y = 45$ deg.

Figure 9 shows dynamic a_n, which is normal to the disc. The time derivative of a_y in the downwind part contributes to the positive time derivative of a_n, while the a_y in the upwind part contributes negatively. Due to strong a_y for the case of Φ_y being 45 deg, the a_n dramatically becomes a steady state as shown in Figure 8c. As the yaw angle increases, the effect of a_y becomes more dominant, particularly for the upwind part.

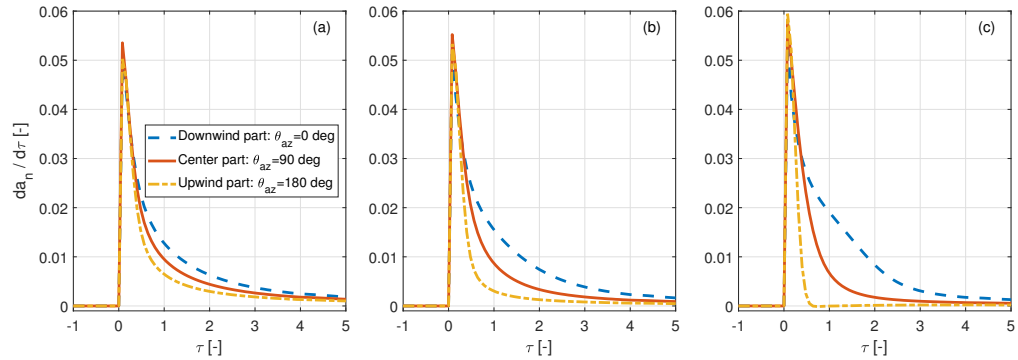

Figure 9. Time derivative of a_n at different azimuth angles from CFD model when base $C_T = 0.6$, step $\Delta C_T = +0.1$, r/D = 0.4, (**a**) $\Phi_y = 15$ deg, (**b**) $\Phi_y = 30$ deg, (**c**) $\Phi_y = 45$ deg.

4.3.2. Radial Position Dependency

Figures 10–12 describe the time derivative of the induction field at different radial positions. For higher r/D, the amplitude of time derivative of a_x, a_y and a_n increases. In particular, on the outside part (r/R > 0.4) of the actuator disc, the time derivative increases dramatically.

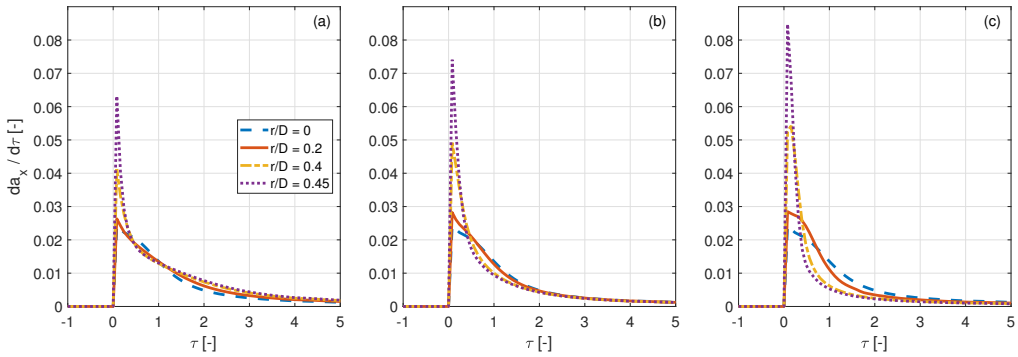

Figure 10. Time derivative of a_x at radial position from CFD model when base C_T = 0.6, step ΔC_T = +0.1, (**a**) downwind part: θ_{az} = 0 deg, (**b**) center part: θ_{az} = 90 deg, (**c**) upwind part: θ_{az} = 180 deg.

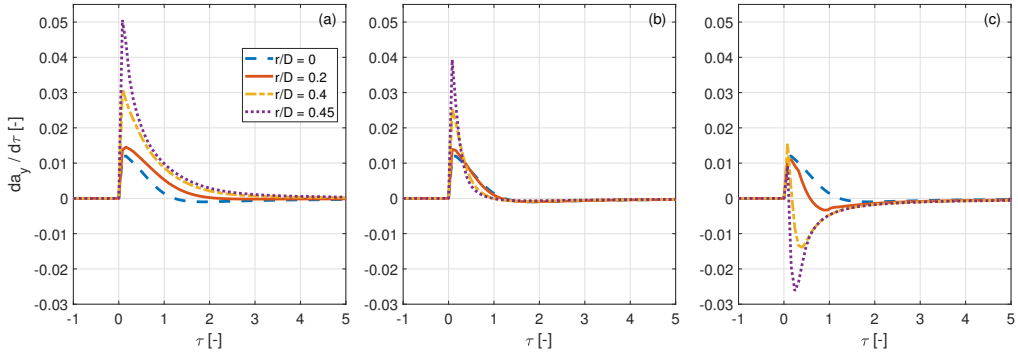

Figure 11. Time derivative of a_y at different radial positions from CFD model when base C_T = 0.6, step ΔC_T = +0.1, r/D = 0.4, (**a**) downwind part: θ_{az} = 0 deg, (**b**) center part: θ_{az} = 90 deg, (**c**) upwind part: θ_{az} = 180 deg.

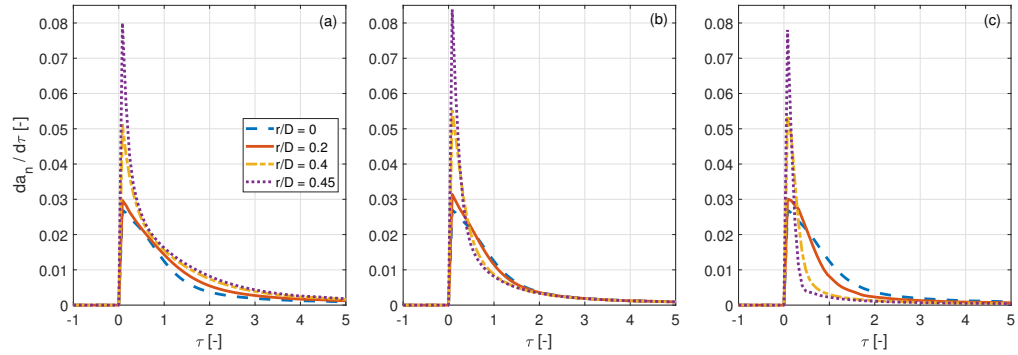

Figure 12. Time derivative of a_n at different radial positions from CFD model when base C_T = 0.6, step ΔC_T = +0.1, r/D = 0.4, (**a**) downwind part: θ_{az} = 0 deg, (**b**) center part: θ_{az} = 90 deg, (**c**) upwind part: θ_{az} = 180 deg.

4.3.3. Thrust Coefficient Dependency

For higher CT, amplitude of $da_n/d\tau$ slightly increases. The effect of the different thrust coefficient is minor for yawed flow as shown in Figure 13.

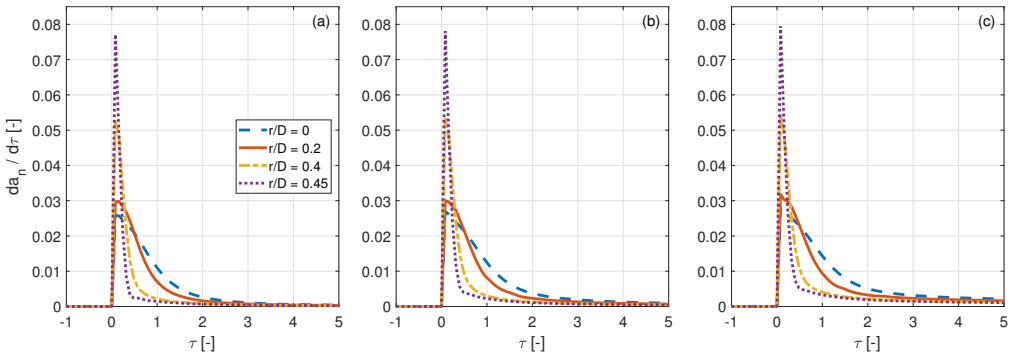

Figure 13. Time derivative of a_n at different radial positions from CFD model, when step ΔC_T = +0.1, θ_{az}= 180 deg, (**a**) Base C_T = 0.2, (**b**) C_T = 0.6, (**c**) C_T = 0.8.

4.3.4. Normalized Induction Field from CFD Results and Modified Dynamic Inflow Models for Yawed Flow at Varying Time Step τ

Normalized induction field from CFD and modified dynamic inflow models for yawed flow are compared in Figures 14 and 15 at varying time step τ. All the dynamic inflow models are coupled with Øye's yaw momentum model since it can predict nonlinear radial dependency for yawed flow among yaw momentum engineering models [8].

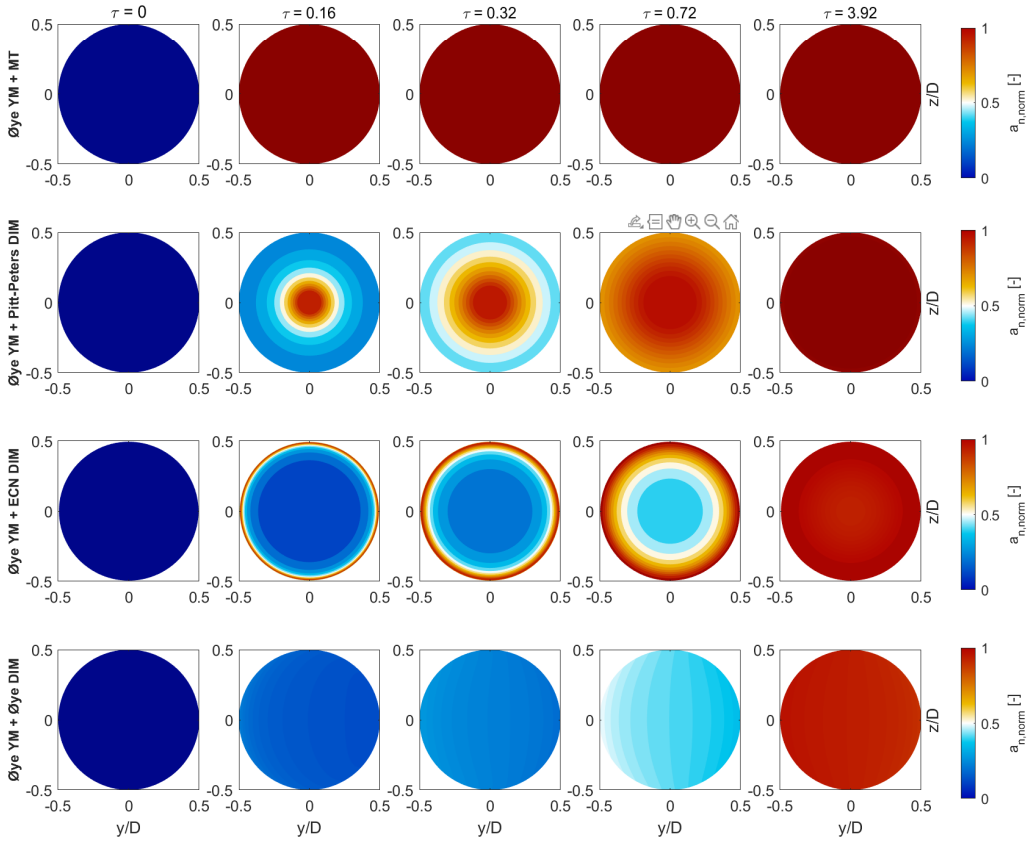

Figure 14. Comparison of normalized induction field $a_{n,norm}$ from different models and τ when base C_T = 0.6, step ΔC_T = +0.1, Φ_y = 30 deg.

The case of steady MT clearly shows the constant step change of the normalized induction field, while all the other models predict non-uniform phase delay. Among all the models, Pitt–Peters DIM and ECN DIM show axis-symmetric normalized induction fields, which implies that those modified models cannot take the yaw effect into account. The asymmetric dynamic phenomena can be described by Øye YM. As explained in

Section 2.1.3, the two linear differential equations enable the model to capture asymmetric phase delay. This model matches best with the CFD model among all the other models for yawed conditions.

Yu pointed out in her work [10] that the Pitt–Peters' dynamic inflow model shows faster phase delay in the center area of the actuator disc, which is physically not correct. The same phenomena occur for the Pitt–Peters DIM.

Yu_PWVM and Yu_FWFM model also can estimate asymmetric trends as shown in Figure 15. At the center of the actuator disc, Yu_FWVM matches well with CFD model. However, at the edge of the actuator disc, Yu_FWFM predicts slower phase delay, while Yu_PWVM shows faster phase delay. In the downwind part, Yu_FWVM shows slower prediction than the upwind part. The azimuth angle dependency in Yu's PWVM and FWVM is less clear than the CFD model, particularly in the early stage of the step load.

The CFD results in Figure 15 describe a clear trend that the phase delay in the upwind part is faster than the phase delay in the downwind part. At the later stage of the step load, the normalized induction field from the CFD model becomes more constant when τ is approximately 4.

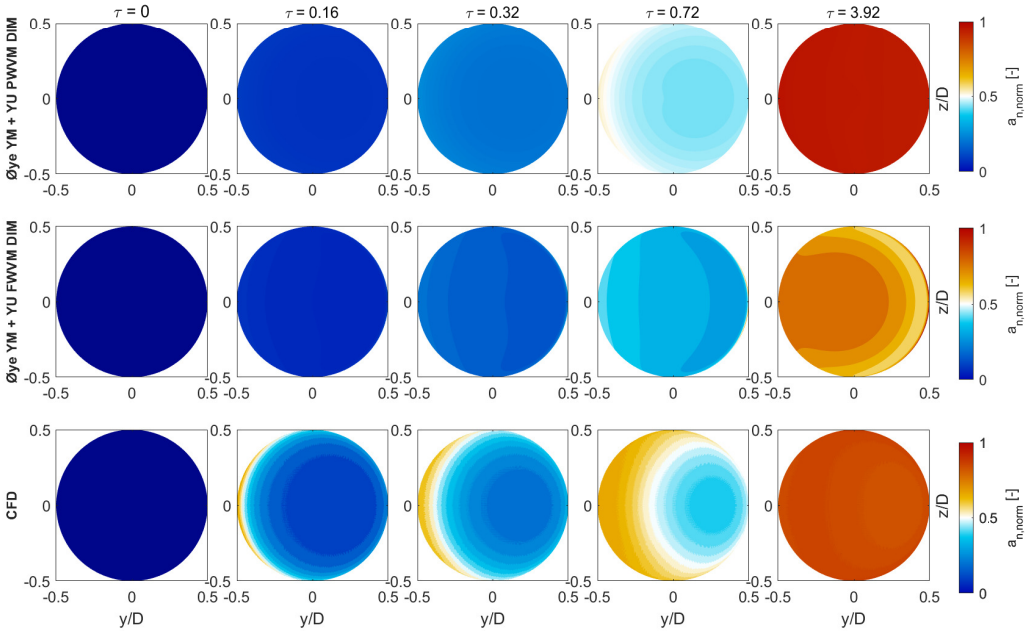

Figure 15. Comparison of normalized induction field $a_{n,norm}$ from different models and τ when base C_T = 0.6, step ΔC_T = +0.1, Φ_y = 30 deg.

Varying τ on the actuator disc are compared to illustrate how fast the overall induction fields from different coupled models change until they reach a certain $a_{n,norm}$, which are 0, 0.1, 0.5, 0.95. Øye's YM + MT clearly shows that it reaches steady state when $a_{n,norm}$ is 0.1 and keep the same τ, and Pitt–Peters and ECN DIM cannot describe asymmetric phase delay as illustrated in Figure 16.

In Figure 17, all the models capture asymmetric trends. In the downwind part, the τ increases faster than the downwind part. However, it is explicit that at the edge of the actuator disc, all the models do not agree with the CFD results well. At the center of the disc, Yu_FWVM matches the best, while the model suffers from significant deficiencies at the edge of the disc, particularly at the early stages. Perhaps the assumption that flow is axis-symmetric cannot be relaxed by coupling yaw models. It is determined that coupling dynamic inflow models and yaw models should be carefully progressed.

It is also recommended that understanding the 3-dimensional wake effect for yawed conditions is significantly important since asymmetric vorticities will cause complex phenomena at the actuator disc.

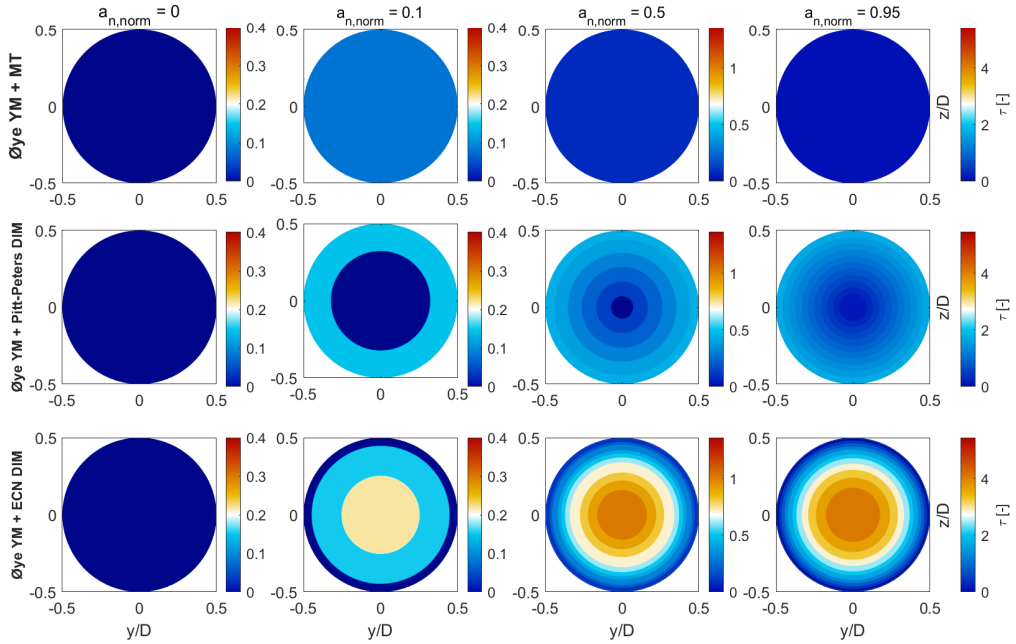

Figure 16. Varying τ at the $a_{n,norm}$ of center = 0.0, 0.1, 0.5, 0.95 from different models when step ΔC_T = +0.1, Φ_y = 30 deg.

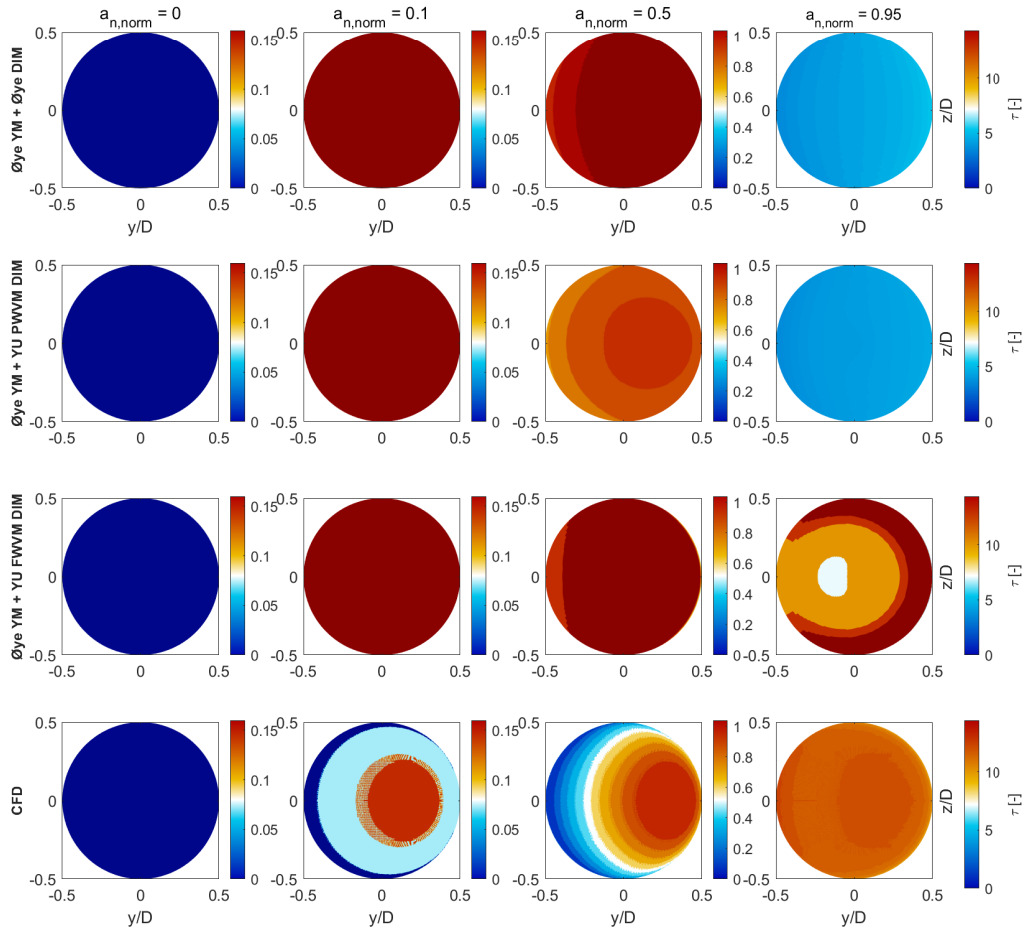

Figure 17. Varying τ at the $a_{n,norm}$ of center = 0.0, 0.1, 0.5, 0.95 from different models when step ΔC_T = +0.1, Φ_y = 30 deg.

5. Conclusions

In this paper, current dynamic inflow models in yawed conditions are evaluated by comparing them with the high fidelity CFD model. Current dynamic inflow models are coupled with steady yaw engineering models to relax the assumption of axis-symmetric flow. Coupling approaches are suggested by applying Glauert's modified momentum theory to dynamic inflow models.

Step responses for yawed flow are analyzed to investigate azimuth, yaw angle, radial position and thrust coefficient dependency. It is clear that the time derivative of a_x and a_y shows different phase delay in the upwind and downwind parts at varying azimuth, yaw, and radial positions, while the effect of the different thrust coefficient is minor. In particular, the time derivative of a_y shows a contrasting trend in the upwind and downwind parts, resulting in significant change in the time derivative of a_n.

Among all coupled models, Øye, Yu PWVM and Yu FWVM DIM can capture asymmetric trends. However, the results show significant deficiencies on phase delay. This indicates that a new dynamic inflow model for yawed flow is necessary.

Author Contributions: Conceptualization, C.H. and C.F.; methodology, C.H.; software, C.H.; validation, C.H.; formal analysis, C.H.; investigation, C.H., C.F. and G.S.; resources, C.H.; data curation, C.H.; writing—original draft preparation, C.H.; writing—review and editing, C.H., C.F. and G.S.; visualization, C.H.; supervision, C.F. and G.S.; project administration, C.F. All authors have read and agreed to the published version of the manuscript.

Funding: This work was supported by the Korea Institute of Energy Technology Evaluation and Planning(KETEP) and the Ministry of Trade, Industry & Energy(MOTIE) of the Republic of Korea (No. 20213040020060).

Data Availability Statement: Not applicable.

Conflicts of Interest: The authors declare no potential conflict of interest.

Nomenclature

C_T	Thrust coefficient [-]
Φ_y, θ_{az}	Yaw angle, azimuth angle [deg]
D, R	Diameter of the actuator disc, radius of the actuator disc [m]
U_∞	Free stream wind velocity [m/s]
f_r	Reduced frequency $\left(\frac{\omega R}{U}\right)$ [-]
x, y, z (Cartesian coordinate)	x is on axial direction aligned with free stream velocity [m]
a_x, a_y, a_z, a_n	Induction factors on x axis, y axis, z axis and normal direction to the disc [-]
τ	Non-dimensionalized time $\left(\frac{tU_0}{R}\right)$ [-]
PWVM, FWVM	Prescribed wake vortex model, free wake vortex model
Øye YM	Øye's yaw model
MT	Momentum theory
Pitt-Peters DIM	The Pitt–Peters' dynamic inflow model
ECN DIM	The ECN dynamic inflow model
Øye DIM	The Øye's dynamic inflow model
Yu PWVM DIM	The Yu's linear dynamic inflow model
Yu FWVM DIM	The Yu's non-linear dynamic inflow model

References

1. Fleming, P.; Gebraad, P.M.; Lee, S.; van Wingerden, J.W.; Johnson, K.; Churchfield, M.; Michalakes, J.; Spalart, P.; Moriarty, P. Simulation comparison of wake mitigation control strategies for a two-turbine case. *Wind Energy* **2015**, *18*, 2135–2143.
2. Gebraad, P.M.; Teeuwisse, F.; van Wingerden, J.W.; Fleming, P.A.; Ruben, S.D.; Marden, J.R.; Pao, L.Y. A data-driven model for wind plant power optimization by yaw control. In Proceedings of the 2014 American Control Conference, Portland, OR, USA, 4–6 June 2014; pp. 3128–3134.
3. Rak, B.P.; Pereira, R.S. Impact of the wake deficit model on wind farm yield: A study of yaw-based control optimization. *J. Wind. Eng. Ind. Aerodyn.* **2022**, *220*, 104827.

4. Wise, A.S.; Bachynski, E.E. Wake meandering effects on floating wind turbines. *Wind Energy* **2020**, *23*, 1266–1285.
5. Schepers, J. Engineering Models in Wind Energy Aerodynamics. Ph.D. Thesis, Aerospace Engineering, Delft University of Technology, Delft, The Netherlands, 2012.
6. van Dijk, M.T.; van Wingerden, J.W.; Ashuri, T.; Li, Y.; Rotea, M.A. Yaw-misalignment and its impact on wind turbine loads and wind farm power output. In *Proceedings of the Journal of Physics: Conference Series*; IOP Publishing: Bristol, UK, 2016; Volume 753, p. 062013.
7. Matha, D.; Sandner, F.; Schlipf, D. Efficient critical design load case identification for floating offshore wind turbines with a reduced nonlinear model. In *Proceedings of the Journal of Physics: Conference Series*; IOP Publishing: Bristol, UK, 2014; Volume 555, p. 012069.
8. Hur, C.; Berdowski, T.; Simao Ferreira, C.; Boorsma, K.; Schepers, G. A review of momentum models for the actuator disk in yaw. In Proceedings of the AIAA Scitech 2019 Forum, San Diego, CA, USA, 7–11 January 2019; p. 1799.
9. Rahimi, H.; Hartvelt, M.; Peinke, J.; Schepers, J. Investigation of the current yaw engineering models for simulation of wind turbines in BEM and comparison with CFD and experiment. In *Proceedings of the Journal of Physics: Conference Series*; IOP Publishing: Bristol, UK, 2016; Volume 753, p. 022016.
10. Yu, W.; Tavernier, D.; Ferreira, C.; van Kuik, G.A.; Schepers, G. New dynamic-inflow engineering models based on linear and nonlinear actuator disc vortex models. *Wind Energy* **2019**, *22*, 1433–1450.
11. Berdowski, T. Three-Dimensional Free-Wake Vortex Simulations of an Actuator Disc in Yaw and Tilt. In Proceedings of the 2018 Wind Energy Symposium, Kissimmee, FL, USA, 8–12 January 2018; p. 0513.
12. Pitt, D.M.; Peters, D.A. Theoretical prediction of dynamic-inflow derivatives. In Proceedings of the 6th European Rotorcraft and Powered Lift Aircraft Forum, Bristol, UK, 16–19 September 1980.
13. Snel, H.; Schepers, J. Engineering moles for dynamic inflow phenomena. *J. Wind. Eng. Ind. Aerodyn.* **1992**, *39*, 267–281.
14. Øye, S. A simple vortex model of a turbine rotor. In Proceedings of the Third IEA Symposium on the Aerodynamics of Wind Turbines, ETSU, Harwell, UK, 16–17 November 1989; pp. 1–4.
15. Glauert, H. *A General Theory of the Autogyro*; HM Stationery Office: Richmond, UK, 1926; Volume 1111.
16. Snel, H.; Schepers, J. *Joint Investigation of Dynamic Inflow Effects and Implementation of an Engineering Method*; Netherlands Energy Research Foundation: Petten, The Netherlands, 1995.
17. Yu, W. The Wake of an Unsteady Actuator Disc. Ph.D. Thesis, Delft University of Technology, Delft, The Netherlands, 2018.
18. Pirrung, G.R.; Madsen, H.A. Dynamic inflow effects in measurements and high-fidelity computations. *Wind Energy Sci.* **2018**, *3*, 545–551.
19. Glauert, H. *The Analysis of Experimental Results in the Windmill Brake and Vortex Ring States of an Airscrew*; HM Stationery Office: Richmond, UK, 1926.
20. Sørensen, J.; Shen, W.; Munduate, X. Analysis of wake states by a full-field actuator disc model. *Wind Energy Int. J. Prog. Appl. Wind. Power Convers. Technol.* **1998**, *1*, 73–88.
21. Jiménez, Á.; Crespo, A.; Migoya, E. Application of a LES technique to characterize the wake deflection of a wind turbine in yaw. *Wind Energy* **2010**, *13*, 559–572.
22. Sørensen, J.N. *General Momentum Theory for Horizontal Axis wind Turbines*; Springer: Berlin/Heidelberg, Germany, 2016; Volume 4.
23. Van Kuik, G.; Lignarolo, L. Potential flow solutions for energy extracting actuator disc flows. *Wind Energy* **2016**, *19*, 1391–1406.